Supporting Information

Quinol-Containing Ligands Enable High Superoxide Dismutase Activity by Modulating Coordination Number, Charge, Oxidation States and Stability of Manganese Complexes throughout Redox Cycling

Laura Senft,[a] Jamonica L. Moore,[c] Alicja Franke,[a] Katherine R. Fisher,[a] Andreas Scheitler,[b] Achim Zahl,[b] Ralph Puchta,[b] Dominik Fehn,[b] Sidney Ison,[c] Safaa Sader,[c] Ivana Ivanović-Burmazović[a]*, Christian R. Goldsmith[c]*

[a] - Department of Chemistry, Ludwig-Maximilian-University, Munich, Butenandtstr. 5-13, D 81377 Munich, Germany.

[b] - Department of Chemistry and Pharmacy, Friedrich-Alexander University Erlangen-Nuremberg, 91058 Erlangen, Germany

[c] - Department of Chemistry and Biochemistry, Auburn University, Auburn, AL 36849, USA

Table of Contents

1. ^{17}O NMR measurements

Experimental Details:

In the case of pH 4.0, a buffer was selected that displays the smallest effect of pressure on the pK_a value for the studied pH range. In this context, 60 mM acetate buffer was used and its pressure dependence of pK_a ($\Delta V_a° = -11.2$ cm^3 mol^{-1},[1] was considered in the calculation of the activation volume for the water exchange reaction at the Mn center of complex **2** at pH = 4.0 (for detailed description of the data treatment see below). The temperature-dependence of the ^{17}O-line broadening was studied from 274.2 to 348.2 K. The pressure-dependent experiments were performed at 288 K or 303 K for pH 4.0 or pH 7.4, respectively, at ambient, 2, 30, 60, 90, 120, and 150 MPa pressures. The number of coordinated water molecules was determined via a method described by Gale et al.[2]

General Data Treatment:

The exchange rates of the bound water molecules were determined by the line-broadening technique developed by Swift and Connick.[3] This approach makes use of the relationship between the reduced transverse relaxation rate ($1/T_{2r}$) and the mean lifetime of the coordinated solvent (τ_m), (see Eq. S1),

$$\pi \cdot 1/P_m(\Delta v_{obs} - \Delta v_{solvent}) = 1/T_{2r}$$

$$= 1/\tau_m\{(T_{2m}^{-2} + (T_{2m}\tau_m)^{-1} + \Delta\omega_m^2)/(T_{2m}^{-1} + \tau_m^{-1})^2 + \Delta\omega_m^2) \} + 1/T_{2os}$$

(Eq. S1)

where T_{2m} describes the transverse relaxation time of coordinated water in the inner sphere of the complex in the absence of chemical exchange, ω_m is the difference in resonance frequency of bulk solvent and solvent in the first coordination sphere, $\Delta v_{obs} - \Delta v_{solvent}$ is the difference between the full line widths at half height of the ^{17}O NMR signal of the bulk solvent in the presence (Δv_{obs}) and absence ($\Delta v_{solvent}$) of the paramagnetic compound, P_m is the mole fraction of bound water ($P_m = n_{H2O}$ x [complex]/55.56), and T_{2os} represents an outer-sphere contribution to T_{2r} that arises from long-range interactions of the paramagnetic unpaired electrons of the metal complex with water molecules outside the first coordination sphere. The exchange rate constant between coordinated and bulk solvent, k_{ex}, can accordingly be expressed as the reciprocal residence time of the bound solvent molecule $k_{ex} = 1/\tau_m$. The line-broadening

experiments were performed at complex concentrations which assured a reasonable broadening compared to the aqueous reference (Δv_{obs}-$\Delta v_{solvent}$ > 20 Hz). The separation of the contributing factors in Eq. S1 is achieved by measuring the temperature dependence of the reduced transverse relaxation rate ($1/T_{2r}$). These measurements are, in principle, restricted to a rather small kinetic window between the boiling and freezing points of water. For the studied systems, temperature range from 274.2 to 348.2 K was selected. A contribution of $1/T_{2os}$ to the reduced transverse relaxation rate that would be clearly visible by a changeover to a positive slope at low temperatures (very slow exchange domain, I) was not observed in the available temperature range, and therefore, this term can be neglected in the treatment of the data. Depending on the selected reaction conditions (on pH value), the studied system operated in different exchange regimes (in different exchange domains). In this context, different contributions to the overall Swift – Connick equation must be taken into consideration.

pH 4.0

The dependence of $\ln(1/T_{2r})$ on $1/T$ clearly shows that under condition of pH = 4.0 the studied system operates in the slow exchange regime (domain II, where $1/T_{2r} \cong 1/\tau_m$) with significant contribution from $1/T_{2m}$ at elevated temperatures (Figure S6).

In that case, the values of $1/T_{2r}$ are best described by Eq. S2 and an exponential Arrhenius-type temperature dependence can be applied in the treatment of the bound water relaxation rate $1/T_{2m}$ as given by Eq. S3.

$$1/T_{2r} = 1/\tau_m\{(T_{2m}^{-2} + (T_{2m}\tau_m)^{-1}+\Delta\omega_m^2)/(T_{2m}^{-1}+\tau_m^{-1})^2+\Delta\omega_m^2)\} \tag{Eq. S2}$$

$$1/T_{2m} = 1/T_{2m}^0 \exp(E_m/RT) \tag{Eq. S3}$$

$$k_{ex} = 1/\tau_m = (k_b/hT) \exp\{(\Delta S^{\neq}/R) - (\Delta H^{\neq}/RT)\} \tag{Eq. S4}$$

The dependence of the exchange rate constant (k_{ex}) on temperature variation can be derived from the Eyring equation (Eq. S4). Here the reciprocal residence time, or k_{ex}, depends on the activation parameters for the water exchange process, viz. the activation enthalpy, $\Delta H^{\neq}$ and activation entropy, $\Delta S^{\neq}$. For ω_m, a reciprocal temperature dependence was applied. The hyperfine coupling constant (A/h) serves as a proportionality factor and defines the relationship between temperature variation and chemical shift of the bound water molecule. Eq. S5 gives the mathematical treatment that describes the temperature dependence of ω_m involving (A/h) as proportionality constant.

$$\omega_m = (2\pi g_L\mu_B S(S+1)B)(A/h)/(3k_B T) \tag{Eq. S5}$$

To clarify unambiguously the detailed mechanism of the studied exchange process, ln $(1/T_{2r})$ was measured as a function of pressure at a constant temperature of 288 K as shown in Figure S7. A study of the pressure dependence is principally advisable in the slow exchange domain (II), because of $1/T_{2r} \cong k_{ex}$. The relationship between the applied pressure and the exchange rate constant at a fixed temperature T is described by Eq. S6,

$$k_{ex} = k_{ex}^0 \exp\{(-\Delta V^{\neq}/RT)\, P\} \tag{Eq. S6}$$

where P = pressure.

In view of the fact that the acetate buffer used for the measurements at pH 4.0 shows pressure dependent value of pK_a ($\Delta V_a^{\circ} = -11.2$ cm^3 mol^{-1}),[1] the appropriate changes in pH and with them associated changes in the concentration of $[Mn(H_2qp1)(H_2O)]^{2+}$ on going from 2 to 90 MPa were taken into consideration for the calculation of the corresponding values of $\ln(1/T_{2r})$ according to the Table S1.

pH 7.4

Under conditions of higher pH (7.4), the temperature dependence for $1/T_{2r}$ revealed a changeover to the fast exchange regime (III) as compared to the system studied at pH 4.0. In this case, the relative long T_{1e} for Mn(II) complexes causes T_{2m} contributions to dominate in Eq. S2 with negligible contributions from ω_m. The values of $1/T_{2r}$ were calculated with the assumption of 1 water molecule exchanging at manganese(II) center. The relevant contributions to T_{2r} under such conditions is adequately described by Eq. S7.

$$1/T_{2r} = 1/\{(\tau_m + 1/C(\tau_m^{-1}+T_{1e}^{-1})\} \tag{Eq. S7}$$

$$C = 4/3\pi^2 S(S+1)(A/h)^2 \tag{Eq. S8}$$

where, T_{1e} is the electronic spin relaxation mainly governed by the transient zero field splitting (ZFS) mechanism. From the nonlinear fit of experimental data to Eq. S4 and Eq. S7 (Figure S4), activation enthalpy and activation entropy were determined. To clarify unambiguously the detailed mechanism of the water exchange processes at higher pH, k_{ex} values were measured as a function of pressure. The pressure experiments were performed by measuring the reduced transverse relaxation rates at different pressures and at a constant temperature of 303 K. The exchange rate constants, k_{ex}, at different pressures were obtained as a solution to the reduced Swift-Connick equation (Eq. S7), which is quadratic function with respect to k_{ex}. On the

assumption that pressure dependence of the exchange rate constant is described by Eq. S6, the activation volume, $\Delta V^{\neq}$, can be calculated from the slope of the resulting straight line P versus $\ln(k_{ex})$ (Figure S5).

Determination of the number of coordinated water

In order to determine the inner-sphere hydration state of manganese(II) center, a method described by Gale et al.[2] was employed. They have shown that at field strengths commonly utilized for NMR spectroscopy (B ≥ 7 T) the maximum ^{17}O relaxivity, r_{2max}^{o}, is directly proportional to the number of inner sphere water ligands (n_{H2O}) according to Eq. S9.

$$n_{H2O} = r_{2max}^{o}/510 \qquad \text{(Eq. S9)}$$

Based on the plot of r_2^o as a function of temperature determined for the studied system (Figure 2) and Eq. S9, the number of water coordinated to the Mn(II) center was estimated to be 1.3 and 0.7 for pH = 4.0 and pH = 7.4, respectively.

2. Figures S1 – S23
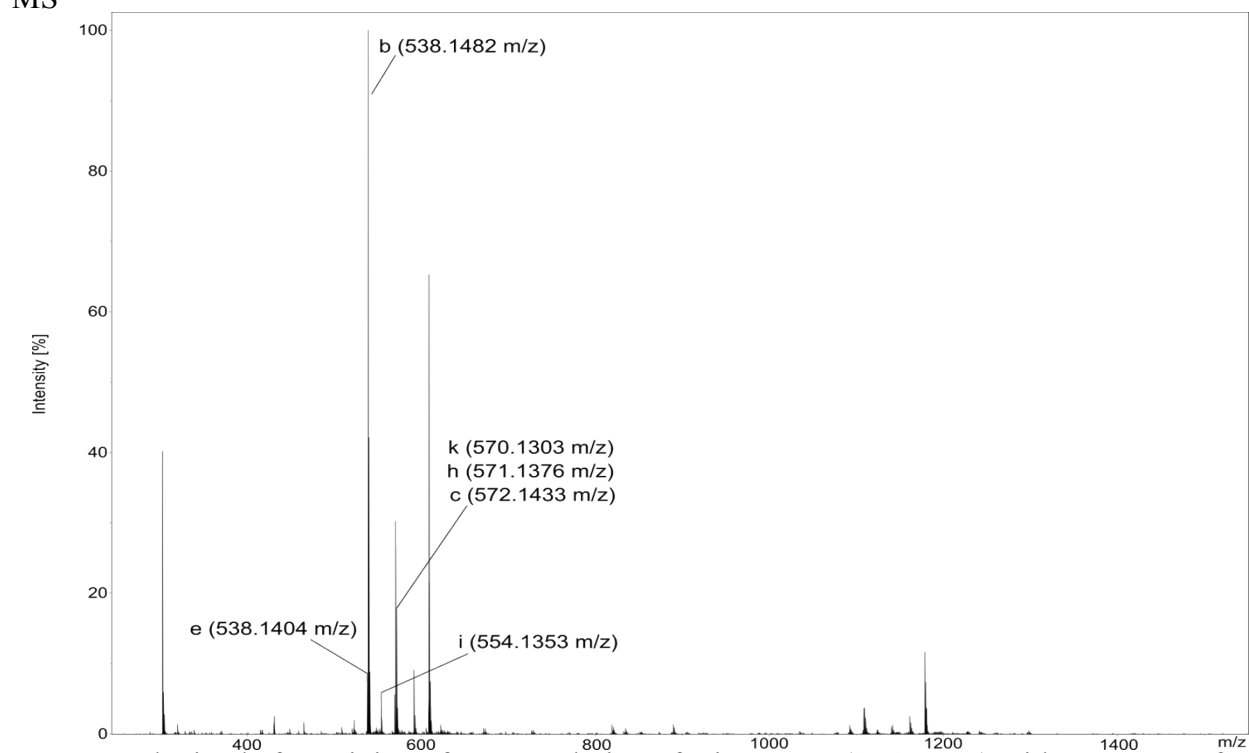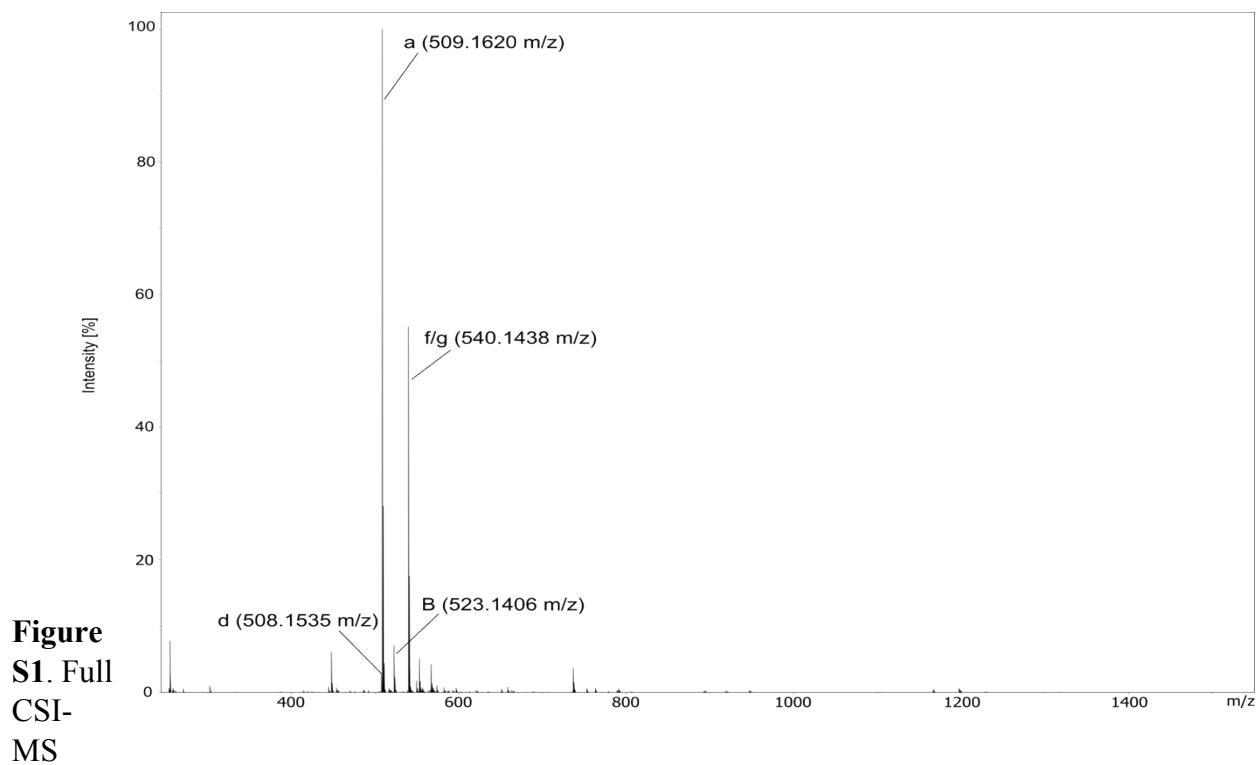
Figure S1. Full CSI-MS spectrum obtained after mixing of 1 mM solution of **2** in MeCN (1 % DMF) with an excess of solid KO_2 at -40 °C. The mixture was diluted with additional MeCN to approximately 1×10^{-5} M and quickly injected into the mass spectrometer.

Figure S2. Full CSI-MS spectrum obtained after mixing of 1 mM solution of **3** in MeCN (1 % DMF) with an excess of solid KO_2 at -40 °C. The mixture was diluted with MeCN to approximately 1×10^{-5} M and quickly injected into the mass spectrometer.
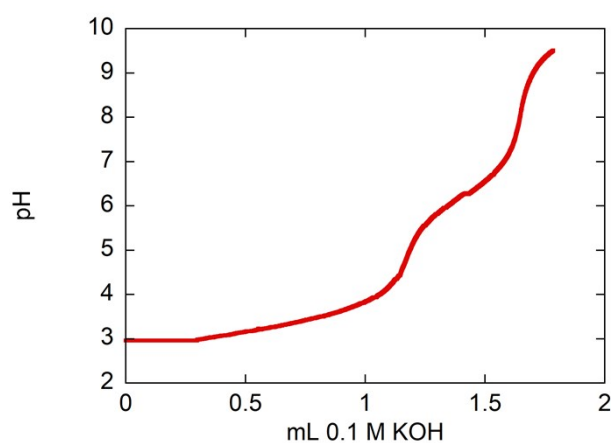
Figure S3. Raw potentiometric pH titration data for the addition of 0.10 M KOH to acidic aqueous solutions containing 100 mM KCl, 1.0 mM H_2qp1, and 1.0 mM $MnCl_2 \cdot (4H_2O)$. Each titration was performed at 25 °C under an argon atmosphere.
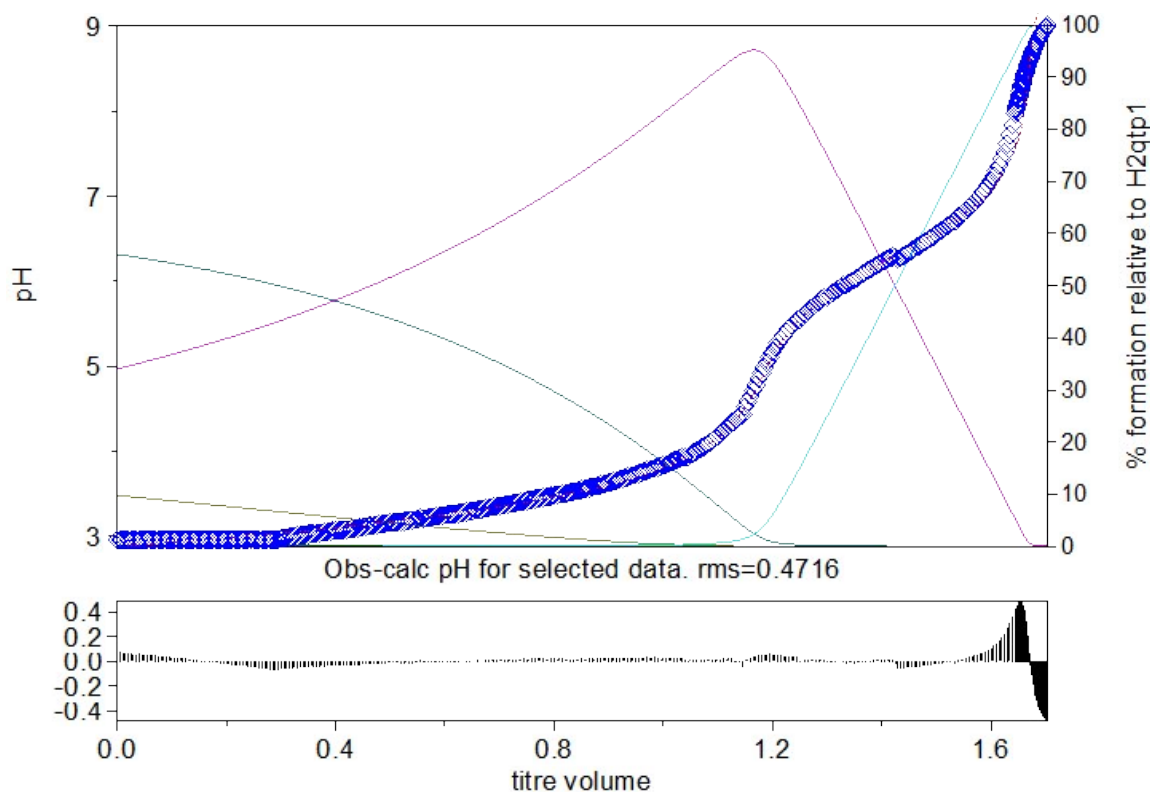
Figure S4. Hyperquad model (red line) overlaid on the experimental data from **Figure S3** (blue). The data above pH 8 have been excluded from the calculations since precipitation was observed above this value. The parameters for the Hyperquad model are provided on Table S2. The residuals for the fit are provided below. The curves represent the formation of various species including $[Mn(Hqp1)]^+$ (light blue), $[Mn(H_2qp1)]^{2+}$ (purple), $[Mn(H_3qp1)]^{3+}$ (pine green), free Mn(II) (olive green).
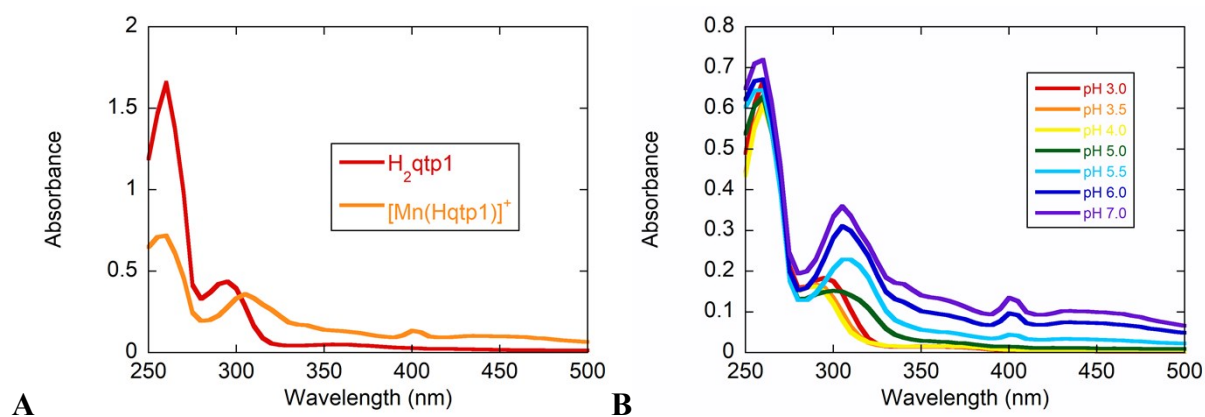
Figure S5. UV/vis data for H$_4$qp2 and **2** in aqueous solutions. All spectra were obtained at 298 K under air using a 1.0 cm pathlength cuvette. A) UV/vis spectra of 0.10 mM solutions of H$_2$qp1 and **2** in aqueous solutions containing 50 mM HEPES buffered to pH 7.00. B) UV/vis spectra of a 0.10 mM solution of **2** in water adjusted to various pH values between 7.0 and 3.0. through the addition of either KOH or HCl.

Figure S6. $(\ln(1/T_{2r}))$ to pH 7.4 Temperature dependence of the reduced transverse relaxation rate for complex **2** in an aqueous 60 mM HEPES solution buffered (see Eq. S4, S7, and S8).
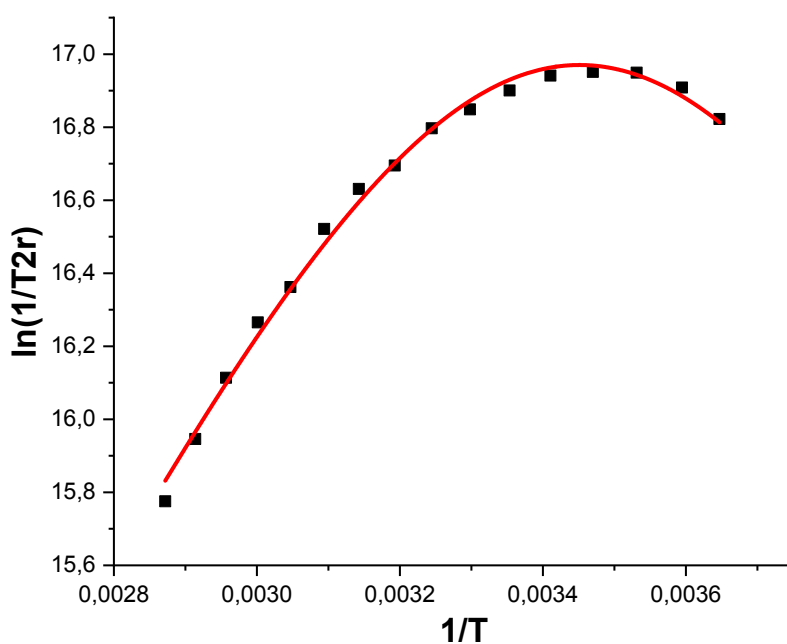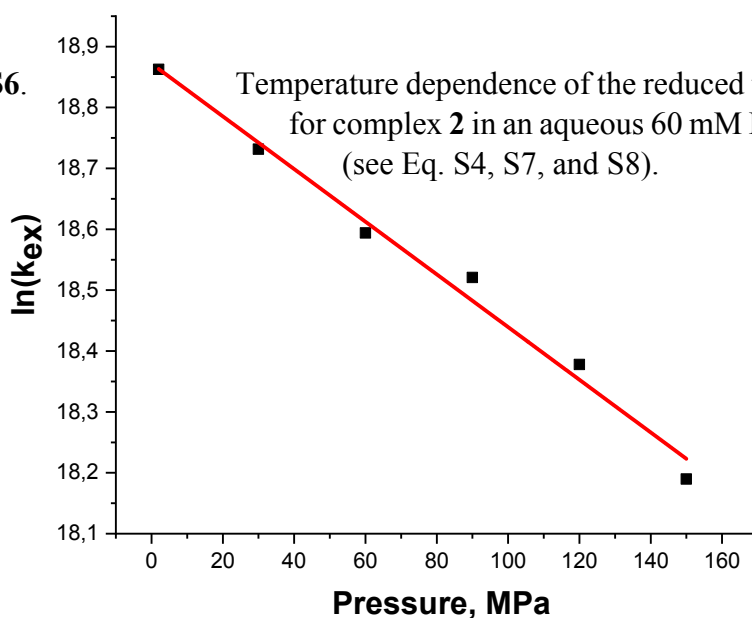
Figure S7. Pressure dependence of ln(k_{ex}) at pH 7.4 and 303 K for complex **2** in an aqueous 60 mM HEPES solution buffered to pH 7.4 (see Eq. S6).
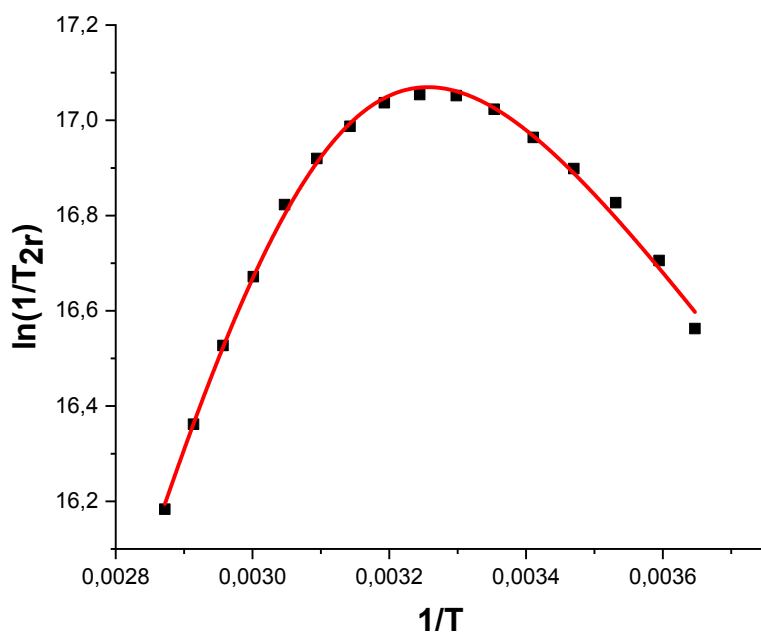
Figure S8. Temperature dependence of the reduced transverse relaxation rate (ln ($1/T_{2r}$)) for complex **2** in 60 mM acetate solution buffered to pH 4.0. The solid line is the result of the nonlinear fit using the reduced Swift-Connick equation (see Eq. S2 – S5).
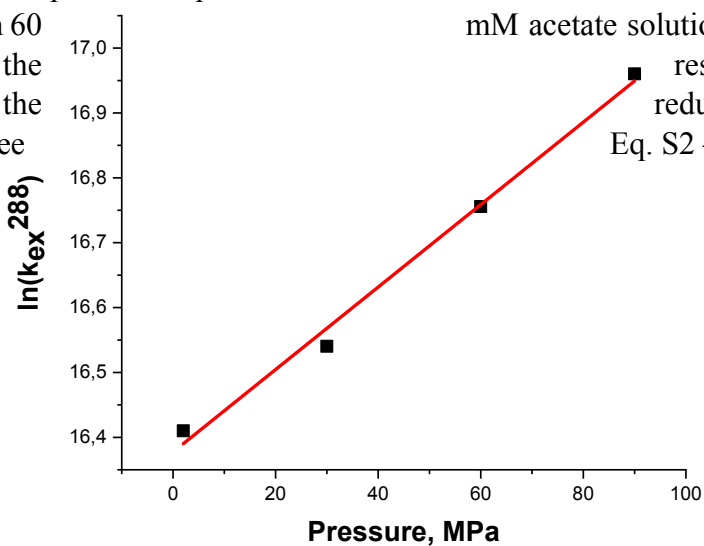
Figure S9. Pressure dependence of $\ln(k_{ex}^{288})$ at pH 4.0 and 288 K for complex **2** in 60 mM acetate buffer (see Eq. S6).
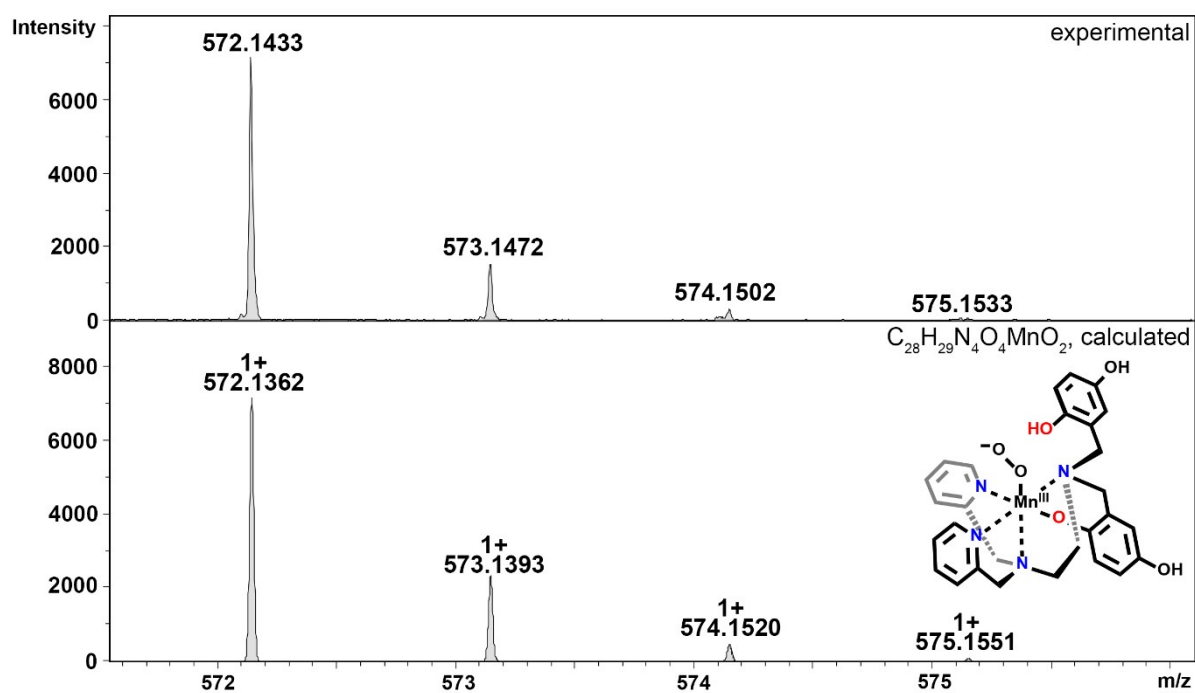
Figure S10. CSI-MS spectrum of **3**. The signal at m/z = 572.1433 is assigned to species **c**, which is $O_2^{·-}$ coordinated to species **b**.
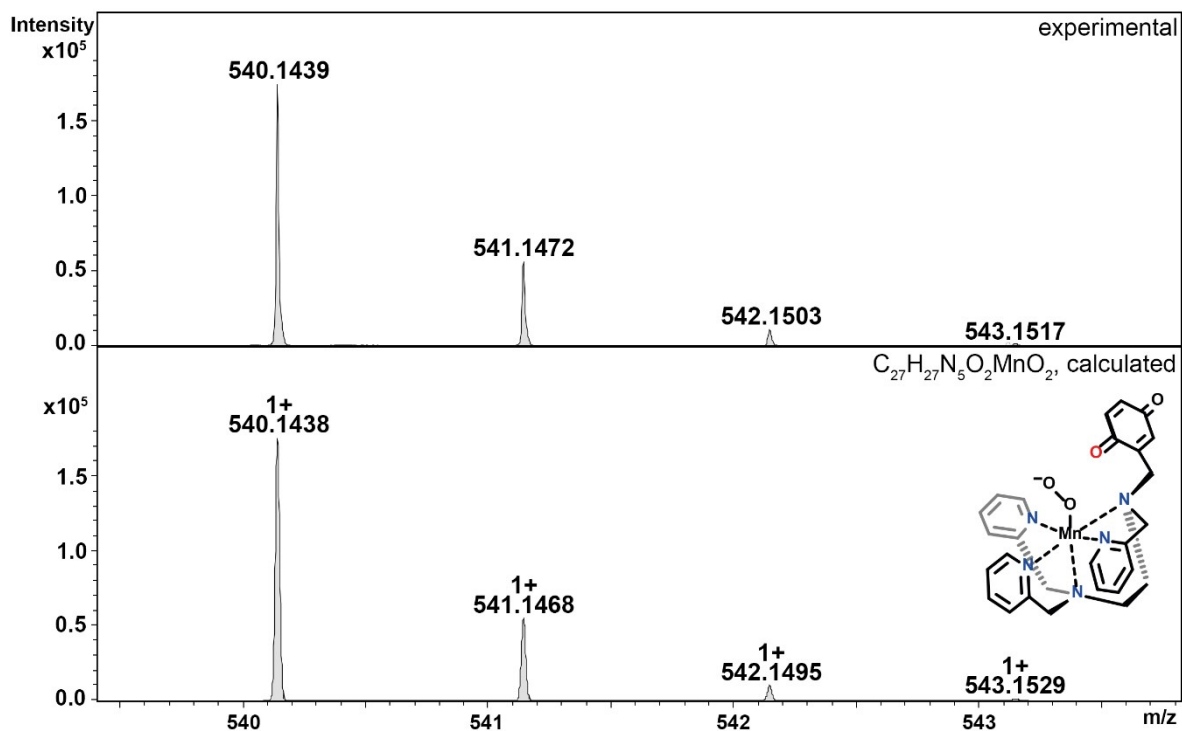
Figure S11. CSI-MS spectrum of the quinone ligand species with Mn(II)-$O_2^{\cdot-}$ $\leftrightarrow$ Mn(III)-O_2^{2-} observed for **2** (**f/g**) at m/z = 540.1439.
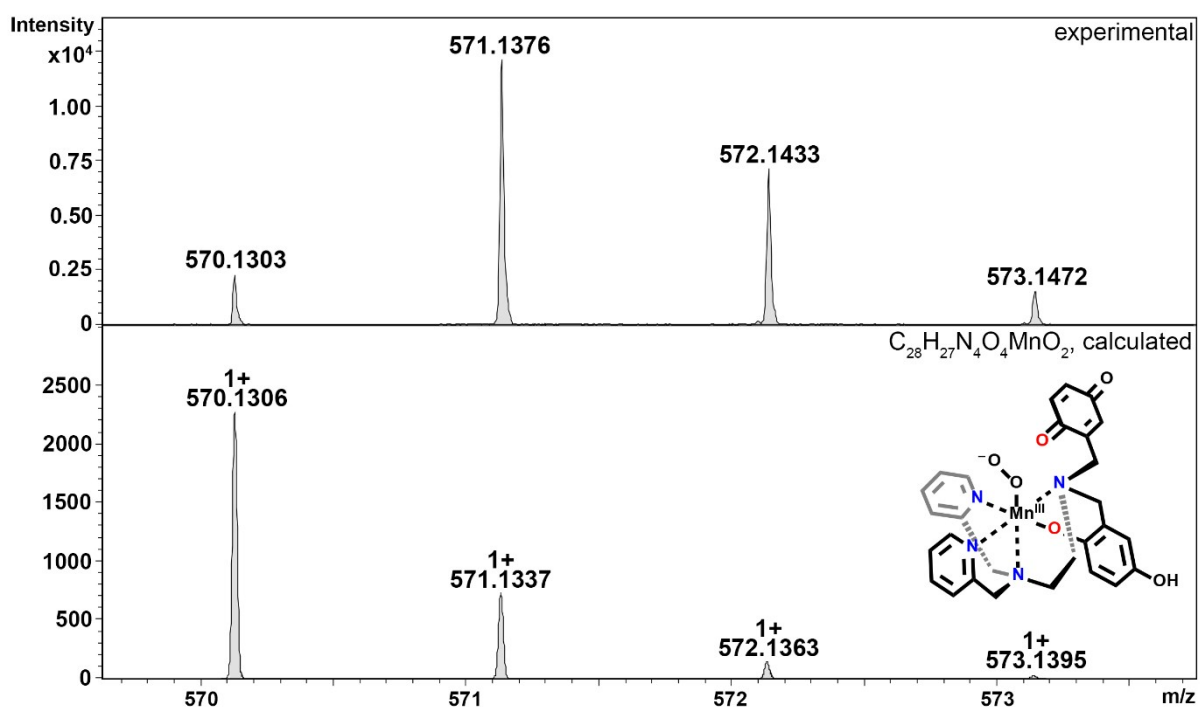
Figure S12. m/z = which is the coordinated to $O_2^{\cdot-}$.

CSI-MS spectrum of **3**. The species at 570.1303 is assigned to species **k**, Mn(III)-quinone complex
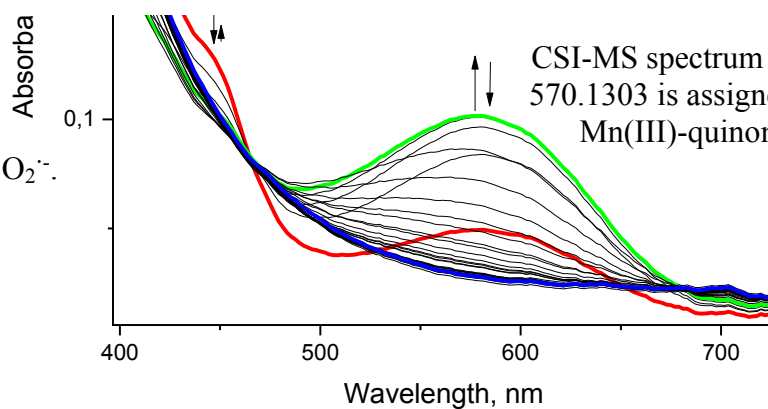
Figure S13. Spectral changes recorded up to 1240 s for the reaction between 1×10^{-4} M **2** and an excess of superoxide in MeCN at -40 °C. Red line: the spectrum recorded immediately after mixing; green and blue lines: the spectra recorded after 30 s and 1240 s, respectively.
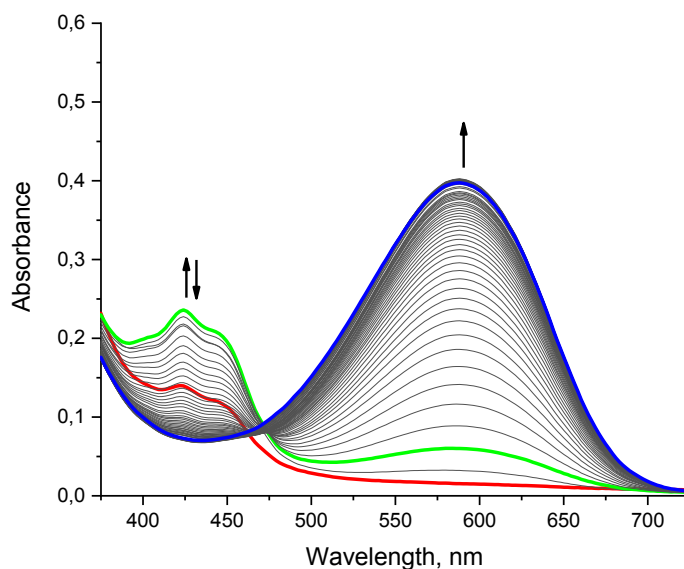
Figure S14. Spectral changes recorded for the reaction between 2×10^{-4} M H$_2$qp1 ligand and an excess of superoxide in MeCN at -40 °C. Red line: the spectrum recorded immediately after mixing; green and blue lines: the spectra recorded after 2 and 62 s, respectively.

Figure S15. Kinetic traces recorded at 590 nm for the reaction of an excess of superoxide with (A) 2×10^{-4} M H$_2$qp1 ligand or (B) 1×10^{-4} M complex **2** in MeCN at -40 °C. The black and red lines correspond to the experimental data and one-exponential fit to the experimental data, respectively.

(A)

(B)

Figure the reaction ligand (red and

$\times 10^{-4}$
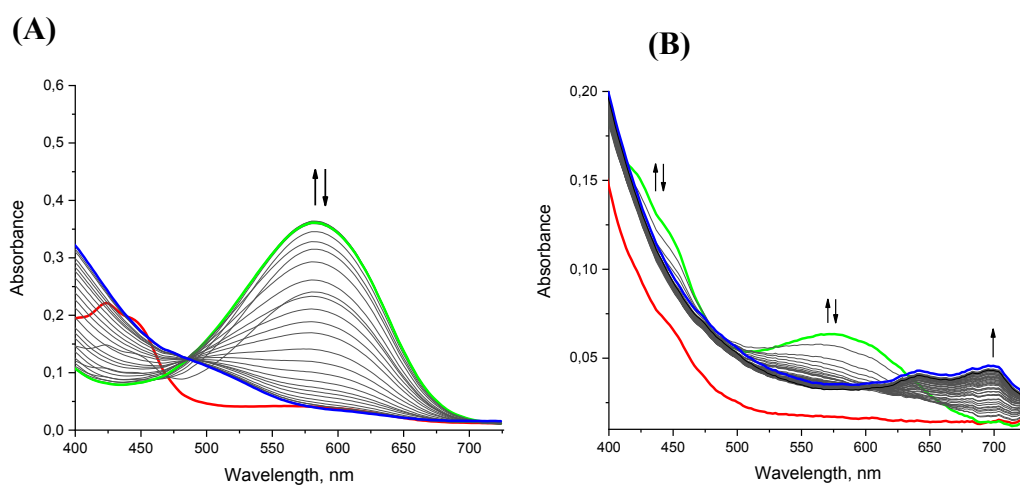
green s,

S16. Comparison of the spectral changes recorded for of an excess of superoxide with (**A**) 2×10^{-4} M H$_2$qp1 line: spectrum taken immediately after mixing; green blue line line: spectrum recorded after 47 and 1240 s, respectively) and (**B**) 1 M **2** (red line: spectrum taken immediately after mixing; and blue lines: spectra recorded after 25 and 1240 respectively) in MeCN at -30 °C.
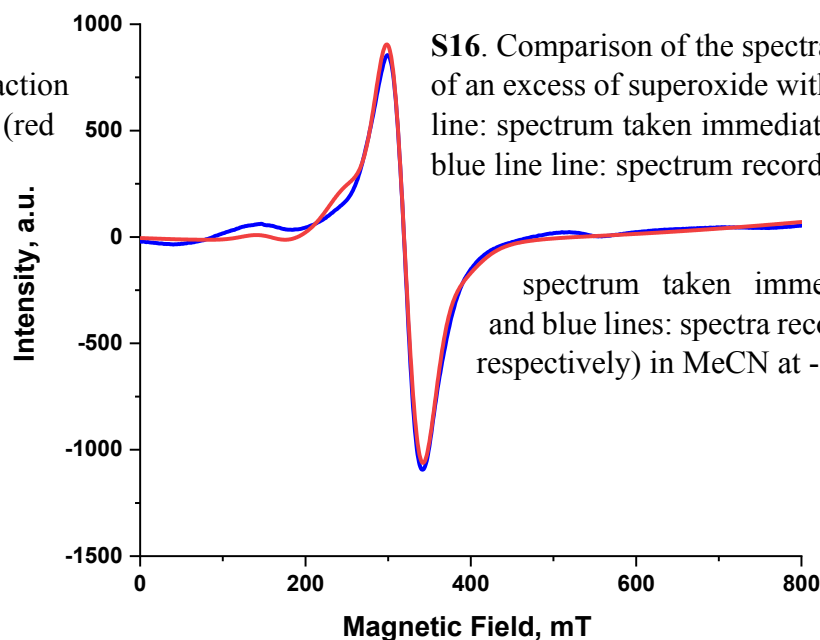
Figure S17. X-band EPR spectrum recorded at 9 K after rapid mixing of 1 mM **2** in CH$_3$CN with an excess of O$_2$·$^-$ at 233 K. 1 equiv. of dibenzo-18-crown-6 was added to solubilize the KO$_2$ in MeCN. Blue line: experimental data; red line: spectrum simulated using EasySpin program[4] (see Table S3 for the values of fit parameters). Experimental conditions: microwave frequency v = 8.959 GHz, modulation width = 0.5 mT, microwave power = 1.0 mW, modulation frequency = 100 kHz, time constant = 0.1 s.
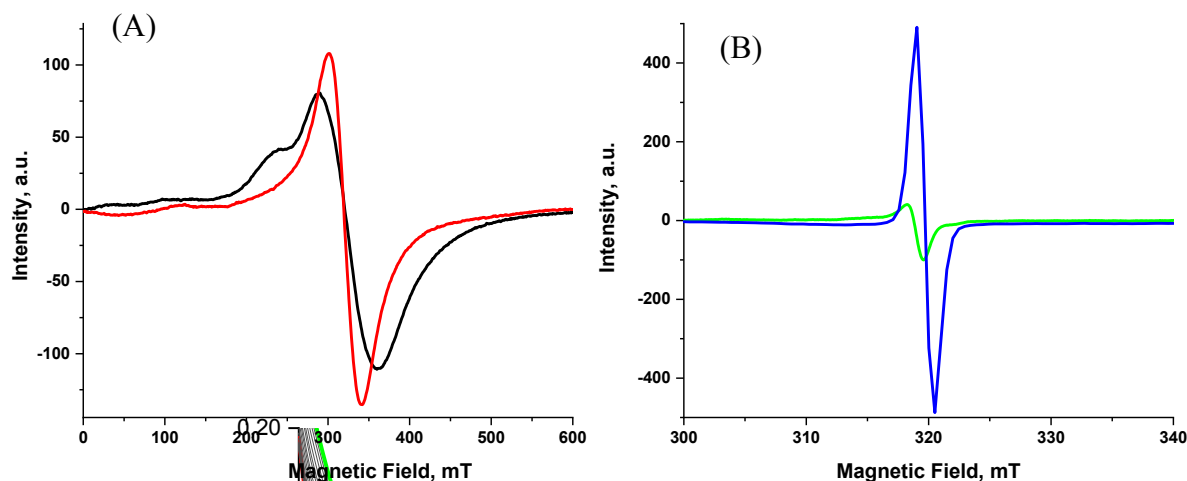
Figure S18. X-band EPR spectra of (A) 0.5 mM **2** in CH$_3$CN (black line) and 0.5 mM **2** after addition of an addition of excess O$_2$·$^-$ (red line) and (B) 0.5 mM H$_2$qp1 after recorded at 95 excess of O$_2$·$^-$ (blue line) and O$_2$·$^-$ in CH$_3$CN (green line) 8.959 GHz, K. Experimental conditions: microwave frequency v = power = 1.0 modulation width = 0.5 mT, microwave constant = 0.1 s. mW, modulation frequency = 100 kHz, time
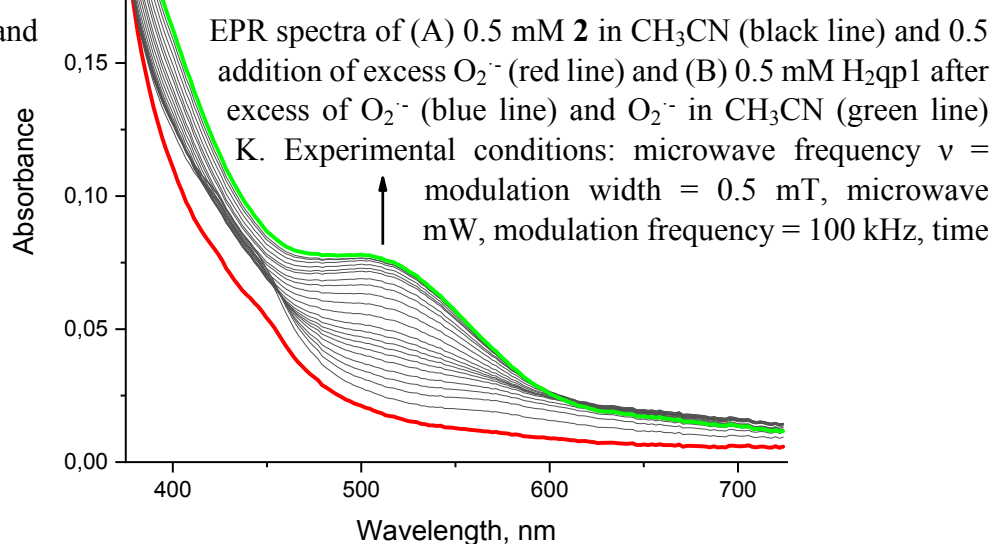
Figure S19. Spectral changes recorded for the reaction between 2×10^{-4} M H$_4$qp2 ligand and an excess of superoxide in MeCN at -40 °C. Red line: the spectrum recorded immediately after mixing; green line: the spectrum recorded after 62 s.
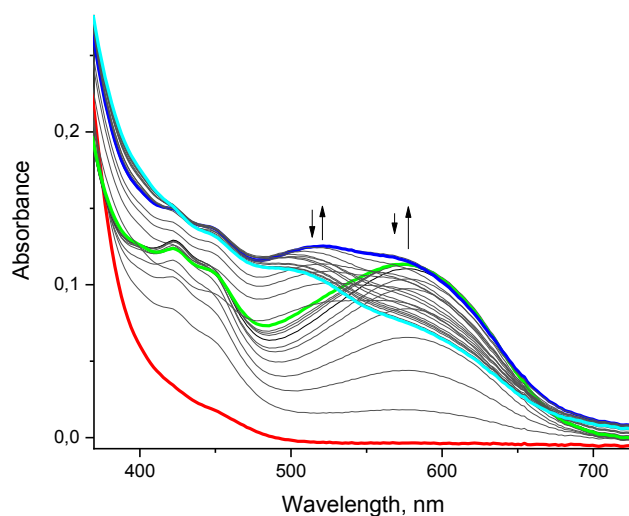
Figure S20. Spectral changes recorded up to 1240 s for the reaction between 1×10^{-4} M **3** and an excess of superoxide in MeCN at -40 °C. Red line: the spectrum recorded immediately after mixing; green, blue, and cyan lines: the spectra recorded after 60 s, 400 s, and 1240 s, respectively.
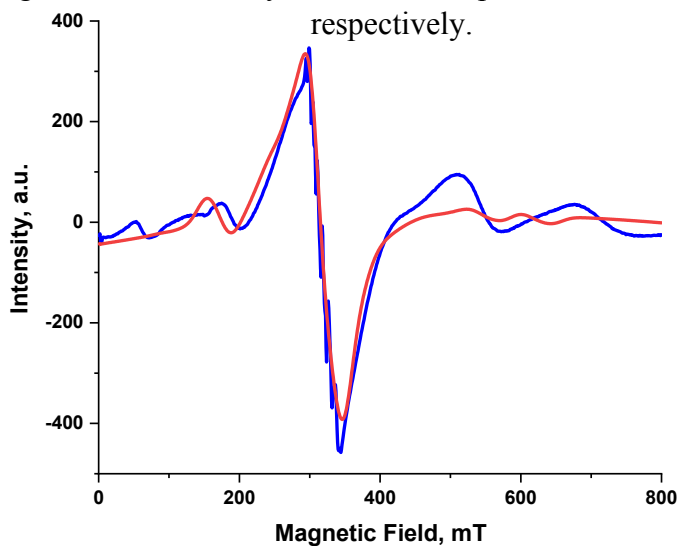
Figure S21. X-band EPR spectrum recorded at 9 K after rapid mixing of 1 mM **3** in CH_3CN with an excess of $O_2{}^{\cdot-}$ in CH_3CN (1 equiv. of dibenzo-18-crown-6 was added to solubilize the KO_2 in MeCN) at 233 K. The reaction was provided 30 s to complete. Blue line: experimental data; red line: spectrum simulated using EasySpin program[4] applying the model with two components, an Mn(IV) species (S=3/2) and an Mn(II) species (S=5/2) (see Table S3 for the values of fit parameters). Experimental conditions: microwave frequency ν = 8.959 GHz, modulation width = 0.5 mT, microwave power = 1.0 mW, modulation frequency = 100 kHz, time constant = 0.1 s.

Figure S22. X-band EPR spectrum recorded at 9 K after rapid mixing of 1 mM **3** in CH_3CN with an excess of $O_2{}^{\cdot-}$ at 233 K and then cooled to 9 K after delay of 10 s. The intense, sharp signal centered at g ~ 2 can be attributed to the presence of superoxide that was not consumed within 10 s of the catalytic cycle. Experimental conditions: microwave frequency ν = 8.959 GHz, modulation width = 0.5 mT, microwave power = 1.0 mW, modulation frequency = 100 kHz, time constant = 0.1 s.

Figure S23. X-band EPR spectrum recorded at 9 K after rapid mixing of 1 mM **3** in CH_3CN with an excess of $O_2{}^-$ at 233 K. The reaction was provided 30 s to complete. Blue line: experimental data; red line: spectrum simulated using EasySpin program[4] applying the model with two components being two Mn(IV) species: one with a $2|D| << h\nu$ and another with a D value greater than $h\nu$ (see Table S3 for the values of fit parameters). Experimental conditions: microwave frequency $\nu = 8.959$ GHz, modulation width = 0.5 mT, microwave power = 1.0 mW, modulation frequency = 100 kHz, time constant = 0.1 s.

3. Tables S1 – S3

Table S1 Changes in pH, concentration of Mn complex and corresponding $\ln(1/T_{2r})$ induced by pressure increase.

Pressure MPa	pH	Conc. of $[Mn(H_2qp1)(H_2O)]^{2+}$ mM	$\ln(1/T_{2r})$
2	4.0	3.00	16,626
30	3.95	2.77	16,906
60	3.91	2.59	17,179
90	3.86	2.36	17,449

Table S2. Parameters for the Hyperquad model used in **Figure S4**.

Species	Mn^{2+}	H_4qp2	H^+	$\log(\beta)$	Derived Values
H_2qp1	0	1	0	0.00	
H_3qp1^+	0	1	1	7.24	$pK_{L2} = 7.24$[a]
H_4qp1^{2+}	0	1	2	11.96	$pK_{L1} = 4.72$[a]
$[Mn(Hqp1)]^+$	1	1	-1	4.2	
$[Mn(H_2qp1)]^{2+}$	1	1	0	10.5	$pK_a(Mn(H_2qp1)^{2+}) = 6.3$[b]
$[Mn(H_3qp1)]^{3+}$	1	1	1	13.6	$pK_a(Mn(H_3qp1)^{3+}) = 3.1$[c]

Due to the instability of the ligand at high pH values, we were unable to obtain $\log(\beta)$ values for the Hqp1^{-} and qp1[2-] species.

[a]Ligand pK_a values corresponding to the (de)protonation of the free ligand amine and pyridine groups. $K_{L1} = [H_3qp1^+][H^+]/[H_4qp2^{2+}]$, $pK_{L1} = \log\beta_{012} - \log\beta_{011}$. $K_{L2} = [H_2qp1][H^+]/[H_3qp1^+]$, $pK_{L2} = \log\beta_{011} - \log\beta_{010}$.

[b]$K_a(Mn(H_2qp1)^{2+}) = [Mn(Hqp1)^+][H^+]/[Mn(H_2qp1)^{2+}]$, corresponds to the (de)protonation of the quinol. $pK_a(Mn(H_2qp1)^{2+}) = \log\beta_{110} - \log\beta_{11-1}$.

[c]$K_a(Mn(H_3qp1)^{3+}) = [Mn(H_2qp1)^{2+}][H^+]/[Mn(H_3qp1)^{3+}]$, corresponds to the (de)protonation of a pyridine group. $pK_a(Mn(H_3qp1)^{3+}) = \log\beta_{111} - \log\beta_{110}$.

Table S3. The values of parameters obtained from the simulations of experimental data to models with either one or two components (see **Figures S17**, **S21**, and **S23**) using the program EasySpin.[4]

Complex	Component	S	g	A_{iso} (MHz)	Line width (MHz)	D (cm^{-1})	E/D	$\sigma_{E/D}$	Percentage
2	1	3/2	1.921, 2.101, 2.027	138.9	36.4	0.048	0.05	0.03	100%
3	1	5/2	1.939, 2.162, 2.000	225.5	23.2	0.032	0.171	0.041	49%
	2	3/2	2.005, 2.005, 2.004	221.8	30.8	0.323	0.031	0.122	51%
3	1	3/2	1.933, 2.146, 1.995	221.5	32.4	0.041	0.160	0.122	58%
	2	3/2	2.001, 2.001, 2.001	224.8	32.6	0.323	0.031	0.122	42%

4. References:

(1)   Neuman, R. C.; Kauzmann, W.; Zipp, A. *J. Phys. Chem.* **1973**, *77*, 2687-2691.

(2)   Gale, E. M.; Zhu, J.; Caravan, P. *J. Am. Chem. Soc.* **2013**, *135*, 18600-18608.

(3)   Swift, T. J.; Connick, R. E. *J. Chem. Phys.* **1964**, *41*, 2553.

(4)   Stoll, S.; Schweiger, A. *J. Magn. Reson.* **2006**, *178*, 42-55.